FEBS Letters 587 (2013) 3792–3801

FEBS Letters

journal homepage: www.FEBSLetters.org

Dynamic expression of miR-126* and its effects on proliferation and contraction of hepatic stellate cells

Can-Jie Guo [a,1], Qin Pan [b,1], Hua Xiong [a], Yu-Qi Qiao [a], Zhao-Lian Bian [a], Wei Zhong [a], Li Sheng [a], Hai Li [a], Lei Shen [a], Jing Hua [a], Xiong Ma [a,*], Jing-Yuan Fang [a,*]

[a] Digestive Disease Laboratory and Department of Gastroenterology, Ren Ji Hospital, School of Medicine, Shanghai JiaoTong University, Shanghai 200001, China
[b] Digestive Disease Laboratory and Department of Gastroenterology, Xinhua Hospital, School of Medicine, Shanghai Jiaotong University, Shanghai 200092, China

ARTICLE INFO

Article history:
Received 30 August 2013
Revised 20 September 2013
Accepted 23 September 2013
Available online 16 October 2013

Edited by Tamas Dalmay

Keywords:
Chronic liver disease
Hepatic stellate cell
miR-126*
VEGFA
Portal hypertension

ABSTRACT

In our previous study, miR-126 was identified as one of the leading miRNAs that is downregulated during activation of hepatic stellate cells (HSCs). However, the roles and related mechanisms of miR-126 in HSCs are not understood. In this study, we compared expression of miR-126 during HSC activation both in vitro and in vivo. We also applied RNA interference to analyze the role and mechanism of miR-126* in the activation of HSCs. Restoring HSCs with Lv-miR-126* resulted in decreased proliferation, accumulation of extracellular matrix components, and cell contraction, while also negatively regulating the vascular endothelial growth factor (VEGF) signal transduction pathways by partially targeted VEGF-A. Thus, we postulate that miR-126 may be a biological marker for the activation of HSCs, and useful for reducing intrahepatic vascular resistance and improving the sinusoidal microcirculation in chronic liver diseases.

1. Introduction

Accumulating evidence suggests that hepatic stellate cells (HSCs) are key players in the pathogenesis of the increased intrahepatic vascular resistance in chronic liver diseases, in which HSCs proliferate, acquire characteristics of contractile cells, and undergo trans-differentiation leading to a myofibroblast phenotype [1,2]. A majority of growth factors and related pathways are involved in the dynamic biological behavior change of HSCs. Among them, vascular endothelial growth factor (VEGF)-A is probably the most important [3]. However, full understanding of HSCs activation is still beyond our reach because of its complexity, especially the intricate regulation of gene expression.

miRNAs are several small non-coding RNAs of 21–25 nt that usually negatively modulate gene expression at the post-transcriptional level by incomplete or complete complementary binding to target sequences within the 3′untranslated region (UTR) of miRNA [4]. Previously, we reported the biological functions and targets of some miRNAs and revealed the signaling pathways regulated by these miRNAs in the activation of HSCs [5,6]. For instance, miR-15 and miR-16 regulate HSC cell growth, apoptosis and proliferation by targeting proteins involved in apoptosis and grow pathways [5,7]. These findings suggest that altered expression of miRNAs may be associated with fibrogenesis, but more studies are required to clarify the mechanism of miRNAs in the development and progression of liver diseases.

In our previous miRNA expression profiling study, miR-126 was downregulated during the activation of HSCs, and appeared to be the most enriched in quiescent stellate cells. Meanwhile, bioinformatics analysis revealed that the VEGF signaling pathway is the most enriched of these differentially upregulated signaling pathways in HSC activation. According to gene ontology (GO) and Kyoto Encyclopedia of Genes and Genomes (KEGG) orthology (KO) analyses, we found that miR-126* is most likely related to the biological behavior of HSCs by partially targeting VEGF-related signaling pathways [5,6]. Here, we demonstrated the dynamic expression of miR-126* in chronic liver diseases, and performed an overall analysis of its effects and its related mechanisms on biological properties of HSCs, on the basis of miRNA expression profile and bioinformatics interpretation. These findings may not only increase our current knowledge about the significance of HSC biological behavior, but also provide a novel therapeutic strategy against intrahepatic vascular resistance in chronic liver diseases.

* Corresponding authors. Address: Shanghai Jiao Tong University School of Medicine, Shanghai Institute of Digestive Disease, 145 Shandong Middle Road, Shanghai 200001, China. Fax: +86 21 63200874.
E-mail addresses: maxiongmd@163.com (X. Ma), jingyuanfang@yeah.net (J.-Y. Fang).
[1] These two authors contribute equally to this work.

0014-5793/$36.00
http://dx.doi.org/10.1016/j.febslet.2013.09.047

2. Materials and methods

2.1. Isolation, culture, and identification of rat HSCs

Primary HSCs were isolated from three normal male Sprague–Dawley rats (400–500 g) by in situ perfusion and density-gradient centrifugation [8]. The rats received humane care according to the Guide for the Care and Use of Laboratory Animals of Shanghai Jiaotong University School of Medicine. All the materials for HSC isolation were obtained from commercial sources as previously described [5].

The isolated HSCs were cultured in Dulbecco's Modified Eagle's Medium, supplemented with 10% fetal bovine serum, 100 U/ml penicillin, 100 mg/ml streptomycin, and 2 mmol/l glutamine. Quiescent and totally activated HSCs were harvested on days 2 and 14. Their purity was detected by immunocytochemistry for desmin (Sigma, St Louis, MO, USA) (1:100). Cell viability was determined by trypan blue staining.

2.2. Animal model of liver fibrosis and histological examination

Thirty-six Sprague–Dawley rats (250–400 g, Laboratory Animals of Shanghai Jiaotong University School of Medicine) were divided into 3 groups of 12 (normal, control, and fibrosis model). Fibrosis model rats were injected subcutaneously with 40% CCl_4 (3 ml/kg, CCl_4:olive oil, 2:3) every 3 days for 8 weeks. Control rats received only olive oil in the same way. Rats were sacrificed at 8 weeks and the degree of liver fibrosis was determined by microscopy. The intra-hepatic HSCs were isolated from CCl_4-induced fibrotic rat livers.

Liver tissues were fixed with 4% formaldehyde in phosphate-buffered saline (PBS) and embedded in paraffin, and 5-μm-thick section were prepared. All the sections were stained with hematoxylin and eosin and standard Van Gieson (VG) staining, which was used to detect collagen fibers. Total RNA from rat HSCs was prepared as described previously [6]. Fibrosis was graded according to the Ishak modified staging system [9]. Histopathology was interpreted by two independent board-certified pathologists who were blind to the study.

2.3. Immunofluorescence staining of HSCs

The expression of VEGFA in quiescent (2 days) and in culture-activated HSCs (14 days) was evaluated by immunocytochemistry. The adherent HSCs were fixed with 4% paraformaldehyde and permeabilized with 0.1% Triton X-100 (Sigma, St Louis, MO, USA). Following blocking in 10% preimmune goat serum for 2 h, cells were incubated with mouse monoclonal anti-VEGFA (1:100, Santa Cruz, USA) overnight at 4 °C. Then cells were incubated with TRITIC-conjugated donkey anti-mouse IgG (Sigma; 1:100) for 1 h. TRITIC fluorescence were visualized using a fluorescence microscope. The positive cells of three randomly selected areas per slide from three slides was used to calculate the expression of VEGFA in HSCs.

2.4. Double immunostaining on cryosections of rat liver

Double immunostaining on cryosections of rat liver were performed as described [10,11]. Liver tissue from five rats per group were blocked with 0.3% H_2O_2 in methanol for endogenous peroxidase activity. double staining experiments on rat livers for desmin in combination with VEGFA were performed. Immunohistochemical examination was carried out by a researcher blind to the experimental design. The percentage of cells co-expressing VEGF/desmin was determined by counting the number of VEGF-positive cells in desmin-positive cells in three different fields per slide from three slides.

2.5. Lentiviral construction, production and transfection

The precursor miR-126* (pre-miR-126) sequences were obtained from miRBase (http://microrna.sanger.ac.uk/sequences/). The premiR-126 sense and antisense primers were: 5′-GCGAATTC-CAGAGGGCAGCTAGCCCT-3′, 5′- GCGGATCCAAGCCTCACCTGTTCT-3′. Lentivector Expression System was purchased from System Biosciences. Packaging and production of lentivirus were performed according to the manufacturer's protocol. Briefly, we first extracted DNA, then designed PCR primers. The product was amplified by PCR contains a sequence of miRNA precursor, which was confirmed by enzyme digestion and then cloned into into the pCDH-CMV-MCS-EF1-copGFP miRNA expression vector (System Biosciences). The new miRNA expression vectors (pCDH-CMV-MCS-EF1-copGFP-miR-126) and Lentivirus Package plasmid mix (System Biosciences) were cotransfected into 293TN cells with Lipofectamine 2000 (Invitrogen). The culture supernatants were collected, concentrated, and used as a virus stock. The viral titer was determined by counting green fluorescent protein (GFP)-positive cells after transfection.

Primary myofibroblast-like HSCs, which had experienced total activation at day 14 and then divided into a blank group, Lv-GFP group, and Lv-miR-126* group with a multiplicity of infection (MOI) from 10 to 50. For 24 h prior to infection, HSCs were plated in each well of 6-well plates, then infected with recombinant viruses (Lv-miR-126* or LV-GFP) at different MOI of for 6 h at 37 °C, followed by the addition of fresh growth medium. Three days later, all lentiviral vectors expressed enhanced GFP, which allowed for titration and measurement of their infection efficiency in transfected cells.

2.6. Quantitative reverse transcriptase polymerase chain reaction (RT-PCR) analysis of miR-126* and VEGF expression

HSCs from 3 rats per group were isolated from rat livers by perfusion of collagenase and pronase, followed by centrifugation over Nycodenz gradient, as described above. RNA purity and concentration were determined by electrophoresis and a BioPhotometer (Eppendorf AG, Hamburg, Germany). The extracted total RNA of HSCs from the three groups was reverse transcribed into cDNA using ExScriptTM RT reagent Kit (TAKARA, Kusatsu, Japan). Expression of mature miRNA was assayed using stem-loop RT followed by PCR analysis, as previously described [5]. PCR analysis was performed in triplicate for each sample. The relative amount of miRNA was normalized against U6 snRNA and VEGF was normalized against GAPDH, and the fold change was calculated by the $2^{-\Delta\Delta Ct}$ method. Primer sequences were listed in Table 1.

2.7. Detection of VEGF-A pathway by Western blotting

Total proteins were prepared by standard procedures and quantified by the BCA method (Pierce, Rockford, IL, USA). Thirty micrograms of protein per sample were loaded onto a 10% SDS–polyacrylamide gel. After electrophoresis, the protein was transferred onto a polyvinylidene difluoride membrane (Millipore, Billerica, MA, USA) by electro-elution. The membrane was incubated with anti-VEGF-A (1:500; Santa Cruz Biotechnology, Santa Cruz, CA, USA) / phosphoinositide 3-kinase (PI3K; 1:200; Santa Cruz Biotechnology)/AKT (1:200; Santa Cruz Biotechnology)/ CCND1 (1:100; Santa Cruz Biotechnology) antibody overnight at 4 °C and with horseradish-peroxidase-conjugated goat anti-mouse IgG (1:2000; Jackson ImmunoResearch, West Grove, PA, USA) for 2 h at room temperature. After washing, the membrane was

Table 1
Primers used in qRT-PCR.

Gene	Sense primers	Antisense primers
miRNA126*	5′-CATTATTACTTTTGGTACGCG-3′	5′-GTCGTATCCAGTGCGTGTCGTG-3′
U6	5′-GCTTCGGCAGCACATATACTAAAAT-3′	5′-CGCTTCACGAATTTGCGTGTCAT-3′
VEGF-A	5′-TGCAGATCATGCGGATCAAAC-3′	5′-TTTCTCCGCTCTGAACAAGGC-3′
GAPDH	5′-ACCACAGTCCATGCCATCAC-3’	5′-TCCACCACCCTGTTGCTGTA-3′

processed using SuperSignal West Pico chemiluminescent substrate (Pierce) and anti-actin antibody (Santa Cruz Biotechnology) (1:500) as an internal standard.

2.8. Luciferase activity assay

The 3′UTR of rat VEGF-A cDNA containing the putative target site for miR-126* was amplified by PCR and inserted into the pGL3 control vector (Promega, Madison, WI, USA) immediately downstream from the stop codon of luciferase (pGL3-VEGFA-3′UTR). A mutant version of the 3′UTR, with a deletion of 7 bp from the site of perfect complementarity was also generated by the QuikChange II Site-Directed Mutagenesis Kit (Stratagene, La Jolla, CA, USA). For reporter assays, cells were transiently transfected with wild-type or mutant reporter plasmid, firefly and Renilla luciferase activities were measured consecutively by dual-luciferase assays kit (Promega) 24 h after transfection.

2.9. In vitro proliferation and cell cycle assay

Cells were seeded in 96-well plates and cultured for 24 h. Cells were starved for 24 h by replacing the medium with serum-free medium, followed by infection with recombinant viruses (Lv-miR-126* or Lv-GFP) at MOI 50. Cell culture was continued for 24, 48 and 72 h and assessed using the Cell Counting Kit 8 (Dojindo, Kumamoto, Japan). The absorbance value of each well was determined at 450 nm using a microplate reader (Molecular Devices, Tokyo, Japan).

Cells were transfected with Lv-miR-126*. At 72 h after transfection, floating and adherent cells were harvested, combined, and processed. Alternatively, nocodazole (100 ng/ml; Sigma–Aldrich, St Louis, MO, USA) was added and cells were further incubated for 16–20 h before harvesting. The supernatant from each well was combined with cells harvested from each well by trypsinization. Cells were collected by centrifugation, fixed with ice-cold 70% ethanol, washed with PBS, and resuspended in 0.5 ml PBS containing propidium iodide (0.5 mg/ml in PBS with 0.1% sodium azide, pH approximately 7.4) and RNase A (1 mg/ml). After final incubation at 37 °C for 30 min, cells were analyzed using a FACSCalibur flow cytometer (Becton–Dickinson, CA, USA). Data were analyzed using FlowJo software (Tree Star, Ashland, OR, USA).

2.10. Measurement of cytosolic free Ca^{2+} and cell contraction

After incubating in 1 ml Fluo-3/AM (5 μmol/l) at 37 °C for 40 min, the HSCs were washed 3 times with PBS, resuspended, and filtered through a 200-screen mesh, and cells were collected and detected with flow cytometry [12]. Contractility of hydrated

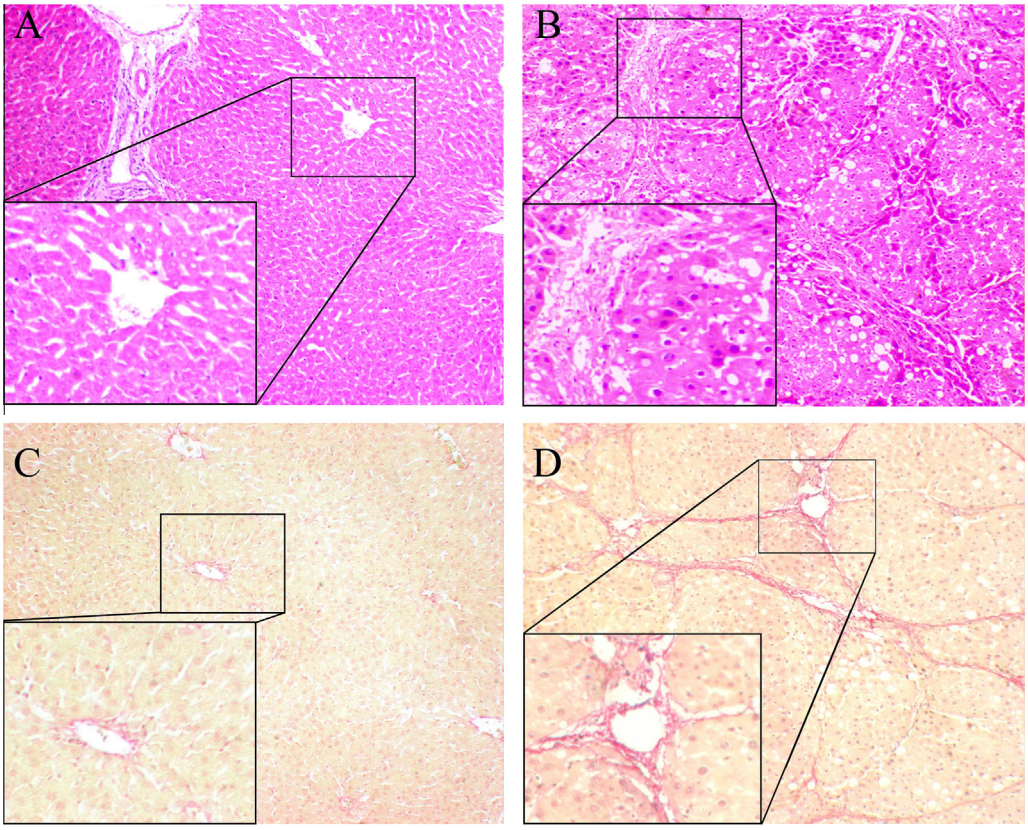

Fig. 1. HE and Van Gieson staining of liver tissue (100×). HE staining of normal and CCl_4-treated liver tissue is shown in panels (A), (B), respectively. Van Gieson staining of normal and CCl_4-treated liver tissue is shown in panels (C), (D), respectively.

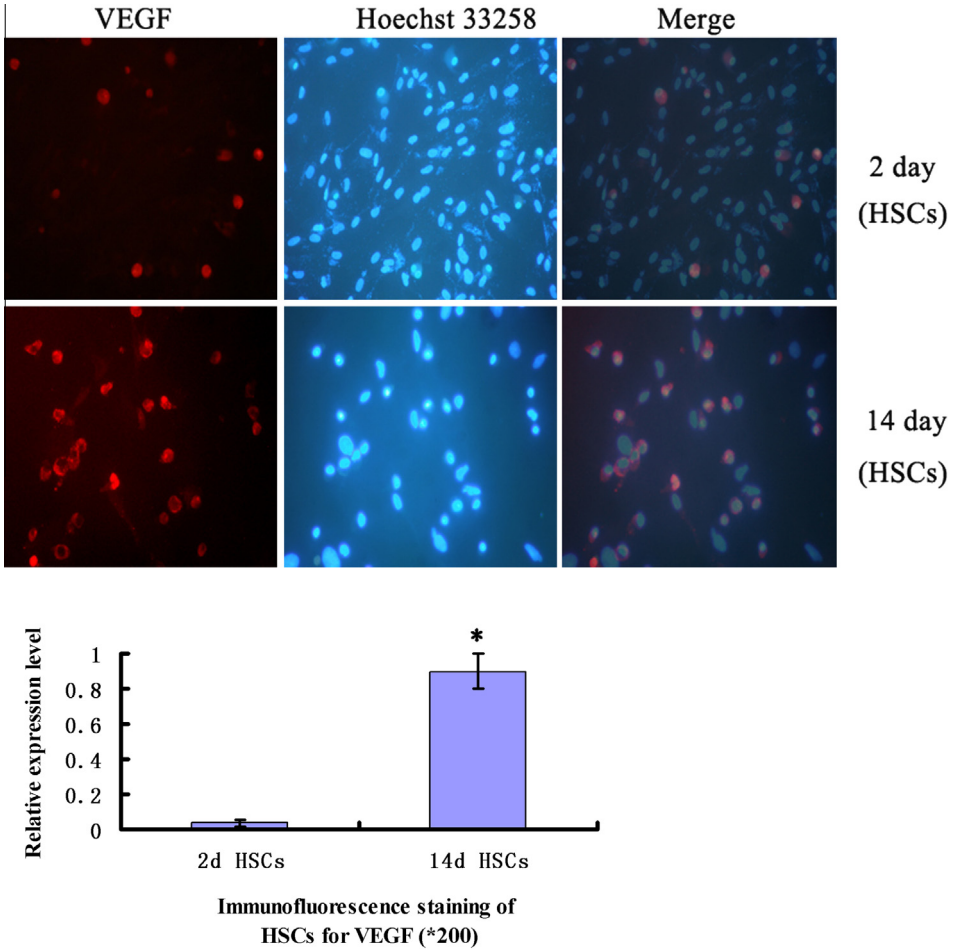

Fig. 2. Immunofluorescence staining of quiescent and activated HSCs for VEGFA (200×). Hoechst 33258 nuclear staining for all conditions is shown in panels.

collagen gels induced by cultured stellate cells was examined according to the method of Rockey and Weisiger [13].

2.11. Enzyme-linked immunosorbent assay (ELISA)

Cells were seeded in 6-well plates and cultured for 24 h. Cells were starved for 24 h by replacing the medium with serum-free medium, and treated with Lv-miR-126* (MOI: 1:50). Cell culture supernatants were collected after 72 h. Hyaluronic acid (HA), laminin (LN), procollagen type III (PC III), and type IV collagen (COL IV) were measured using ELISA kits (R&D Systems Inc, Minneapolis, MN, USA) according to the procedure recommended by the manufacturer.

2.12. Statistical analysis

All the results are expressed as mean ± standard deviation (S.D.). Statistical analysis was performed using the Student's *t* test for comparison of two groups, and analysis of variance for multiple comparisons. In both cases, differences of $P < 0.05$ were considered statistically significant.

3. Results

3.1. In vitro activation of rat HSCs

About 5×10^8 ml^{-1} HSCs were harvested from each rat. The percentage of freshly isolated living HSCs was up to 95% as defined by trypan blue staining. More than 95% of the HSCs showed positive desmin staining on days 2 and 14, indicating high purity of HSCs as previously described [5].

3.2. CCl_4 induced liver fibrosis in rats

Histological examination, classified according to the grade of liver fibrosis, revealed that the degree of liver fibrosis progressed in rats that received CCl_4 relative to rats receiving olive oil alone. Fig. 1 revealed little fibrosis in the liver of normal rats. On the contrary, hepatic steatosis, necrosis and infiltration of inflammatory cells were obvious in the fibrosis model group. Moreover, there was nodular fibrosis with extensive collagen deposition and well-delineated fibrosis septa, which were continuous and extended in each section, sometimes even bridging portal regions. In contrast to the normal rats (stage 0), the Ishak staging for the fibrosis model group (10 w) reached 5.4 ± 1.0.

3.3. Differential expression of miR-126* and VEGF-A during HSC activation both in vivo and vitro

Intrahepatic HSCs were isolated from rat liver with CCl_4-induced experimental fibrosis, and then subjected to both Quantitative RT-PCR and dual-immunofluorescent staining. Being evaluated by these two assays both in vivo and vitro (Figs. 2–4), the VEGF expression was virtually undetectable in quiescent HSCs. However, dramatic increase of VEGF level occurred in HSCs after their activation both in vivo and vitro ($P < 0.05$). This result was vice versa for

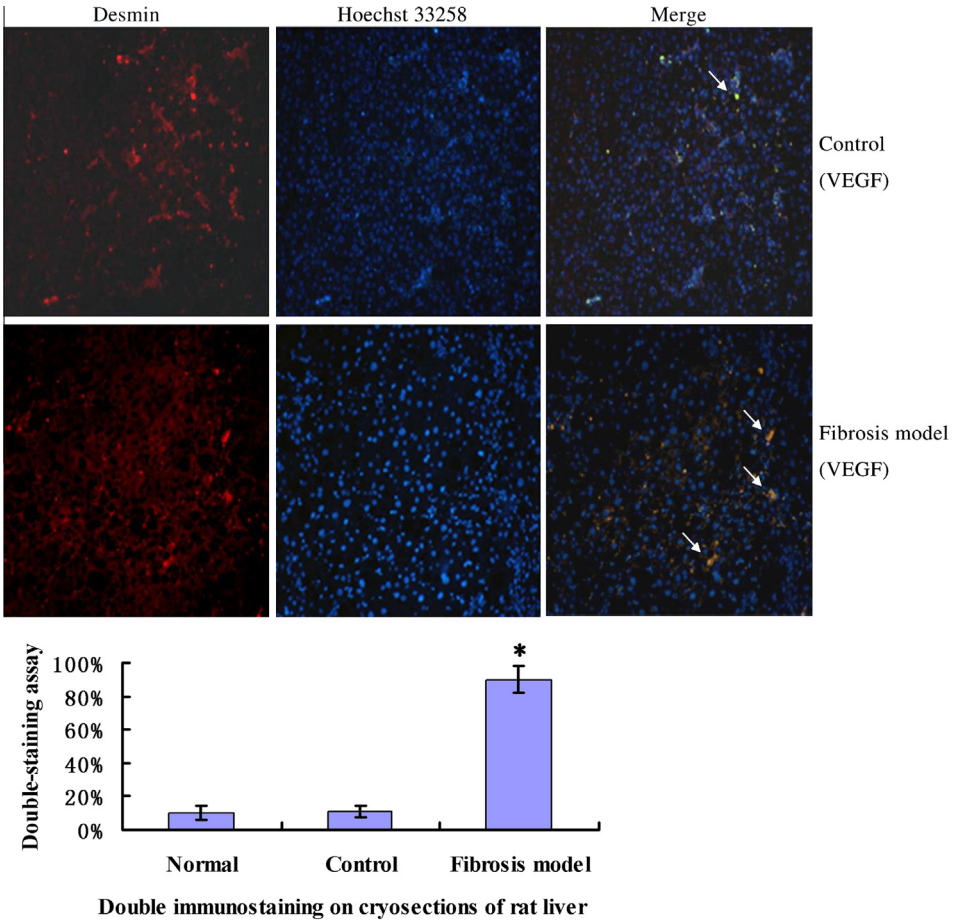

Fig. 3. Double immunofluorescence staining of VEGFA and desmin in liver tissue.(×200): double staining of desmin (red), VEGF (green) and Hoechst in nuclei (blue) was in the liver tissue. At the arrowheads were the expression of VEGFA in HSCs showing red-green double stained cytoplasm and blue-stained nuclei.

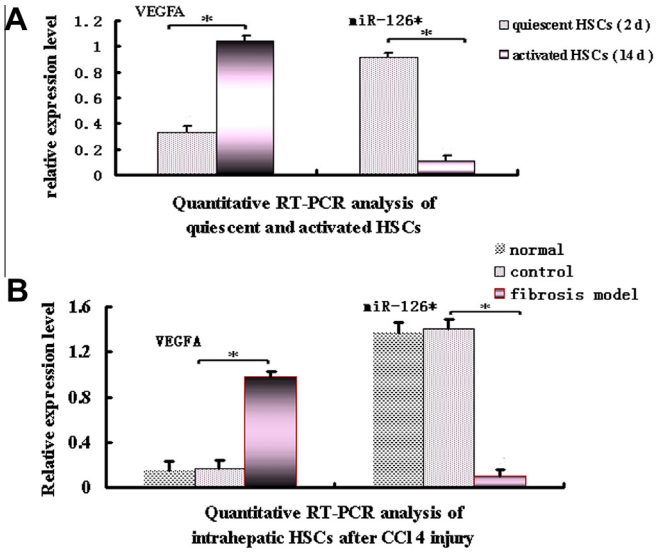

Fig. 4. mRNA relative levels of miR-126* and VEGF-A by quantitative real-time PCR. (A) Relative expression of miR-126* and VEGF-A on days 2 and 14 in vitro. (B) Relative expression of miR-126* and VEGF-A in the intrahepatic HSCs after CCl_4 injury. Statistically significant differences between groups is indicated by $P < 0.05$.

miR-126*, which reduced statistically throughout the HSCs' activation ($P < 0.05$).

3.4. Lentiviral delivery of miR-126*

The recombinant plasmid pCDH-CMV-MCS-EF1-copGFP-miR-126 was confirmed by restriction endonuclease analysis and DNA sequencing. Virus titer was 10^8 > ifu/ml. the efficiency of transfection was estimated by determining the percentage of GFP-positive cells and fluorescence-activated cell sorting confirmed that 99% of HSCs were transduced with Lv-miR-126* (MOI:50). The following assays were done with Lv-mediated gene transfer at MOI 50.

3.5. Effect of miR-126* on inhibition of VEGF expression and inactivation of PI3K/AKT pathway

Examination of the homology between rno-mir-126* and VEGF-A mRNA sequences showed that the 7 nucleotides in the seed region of miR-126* were complementary to bases 3380–3386 of VEGF-A 3′UTR (NM_031836.2). Thus an inhibitory effect of miR-126* on VEGF-A was inferred.

HSCs treated with Lv-miR-126* at MOI 50 for 72 h, and the expression of miR-126* increased significantly. To investigate further the actions of miR-126* on VEGF-A, we investigated the expression of VEGF-A at the mRNA and protein levels. mRNA level

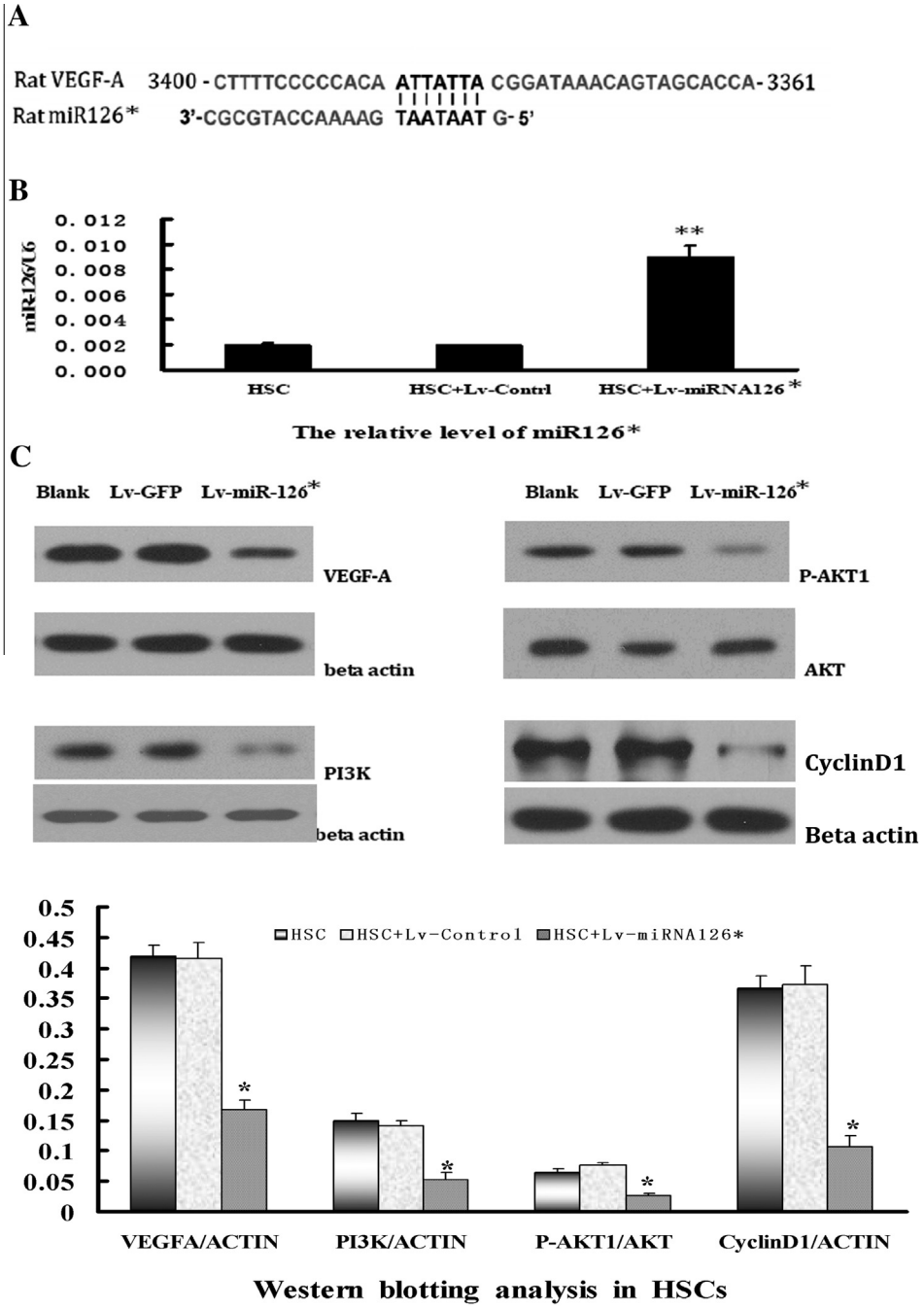

Fig. 5. (A) VEGF-A is the target of miR-126*. miR-126* shares the conserved binding sites in VEGF-A 3′UTR. The site of target mutagenesis is indicated. (B) mRNA levels of miR-126* in HSCs analyzed by quantitative real-time PCR. (C) Protein levels of the VEGF-A/PI3K/AKT/CCND1 pathway detected by Western blotting. Data are expressed as means ± S.D. of 3 observations. $^{*}P < 0.05$, $^{**}P < 0.01$ versus corresponding control using Student's *t* test.

showed no difference but the protein level was downregulated significantly compared with those in the controls ($P < 0.05$). Western blotting also showed that restored Lv-miR-126* reduced its downstream protein expression, including PI3K, phospho-AKT (p-AKT) and CCND1 (cyclin D1), which is considered to play an important role in the biological behavior of HSCs (Fig. 5).

To assess further whether miR-126* directly regulated VEGF-A expression through the target site at the 3′-UTR of VEGF-A mRNA, we used a luciferase reporter assay. A significant decrease in relative luciferase activity was noted when pGL3-VEGFA 3′UTR was cotransfected with miR-126*. In contrast, the inhibitory effect was abolished by partial deletion of the perfectly complementary sequences in the VEGF-A 3′-UTR (pGL3-mutVEGFA-3′-UTR), which disrupted the interaction between miR-126* and VEGF-A (Fig. 6).

3.6. Effects of upregulated expression of miR-126 on proliferation and contraction of HSCs*

To verify whether the miR-126* family affected biological behavior of HSCs by regulating the VEGF pathway, we measured cell proliferation using the cell proliferation assay. Fig. 7A shows that inhibition of VEGF-A expression by RNA interference

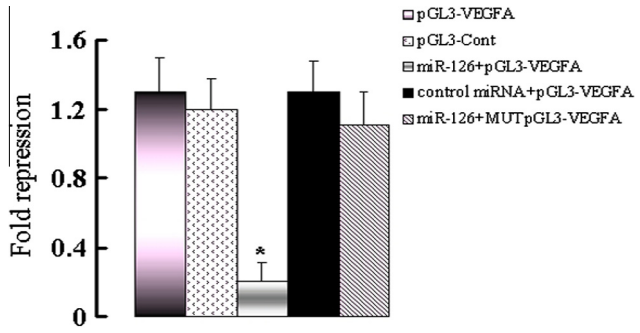

Fig. 6. Dual luciferase assay performed in activated HSCs transfected with luciferase construct alone or cotransfected with Lv-miR-126* or Lv-GFP. Firefly luciferase construct containing mutant (MutpGL3-VEGFA) target site of the VEGF-A 3′UTR was generated and transfected as indicated. Firefly luciferase activity was normalized to Renilla luciferase activity for each sample. The results are expressed as the mean ± S.D. from 3 independent experiments. $^{*}P < 0.01$ compared to corresponding control.

suppressed growth of HSCs. Cell cycle experiments showed that HSCs transfected with miR-126* had increased numbers of cells in G0/G1 phase, corresponding decreases in S phase, but no significant difference in G2/M phase. These results indicate that miR-126* contributed to induction of G0/G1 arrest in HSCs, which was partially through downregulation of the PI3K/AKT/CCND1 pathway (Fig. 7B and C).

The cytosolic free Ca^{2+} and cell contraction were also measured. Intracellular calcium concentration in HSCs was determined by flow cytometry using calcium fluorescent probe Fluo-3/AM. The mean fluorescence intensity (MFI) of Fluo-3/AM in Lv-miR-126* HSCs was 33.20 ± 5.60 and 204.92 ± 20.87 in the control group, which demonstrated that the intracellular calcium concentration in HSCs in the Lv-miR-126* group was significantly decreased ($P < 0.01$) (Fig. 8).

As shown in Fig. 9, when activated HSCs were cultured on collagen gels for 9 days, the diameter of the gels significantly decreased to 34.7 ± 6.5% (mean ± S.D. of 3 wells; $P < 0.05$ vs DMEM alone), The surface of the collagen gels on which stellate cells or Lv-control were plated became obviously concave. On the other hand, Lv-miR-126* addition to the medium significantly inhibited the contraction of collagen gels (17.0 ± 5.2% of the original diameter).

3.7. Effect of miR-126* targeting of VEGF-A on ECM degradation modulators

After treatment with miR-126* for 72 h, the contents of HA, LN, PC III and COL IV in the cell culture supernatant were significantly inhibited compared with the normal and control groups ($P < 0.01$) (Table 2).

4. Discussion

The miR-126 family is known to be associated with angiogenesis, and has been extensively analyzed in tumor cell lines [14,15]. miR-126/miR-126* is located within the egfl7 (epidermal growth factor-like domain 7, EGFL7) gene, which is implicated in vessel development through promoting VEGF signaling, angiogenesis, and vascular integrity. It is also involved in cell-growth regulation in several diseases, such as colorectal cancer, gastric cancer, and liver carcinoma, by regulating multiple target genes including IRS

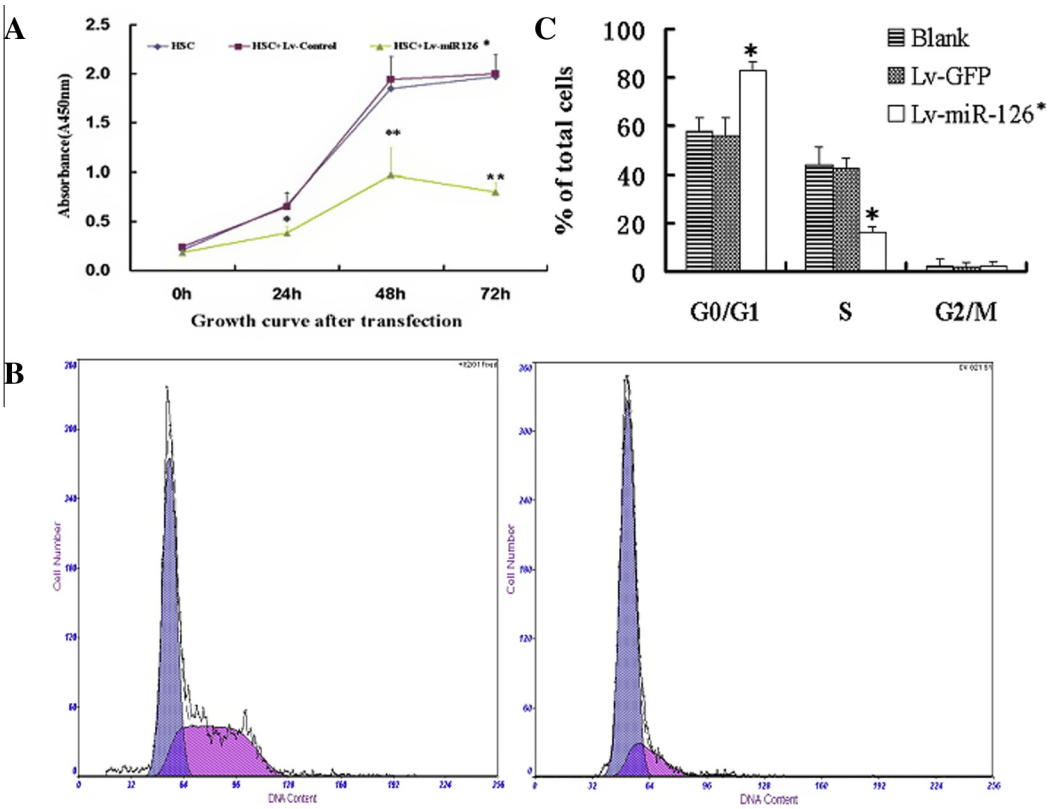

Fig. 7. Inactivation of VEGF-A/PI3k/Akt/CCND1 pathway by miR-126* suppressed proliferation and induced G0/G1 arrest in HSCs. (A) The proliferation curve of HSCs. Cell proliferation was analyzed using CCK-8 cell proliferation assay kits. Each value represents the mean of six replicates. The proliferation of HSCs transfected with LV-miR-126* was suppressed significantly compared with cells that were not transfected or were transfected with control vector. (B and C) HSCs cell cycle was analyzed by FACS.

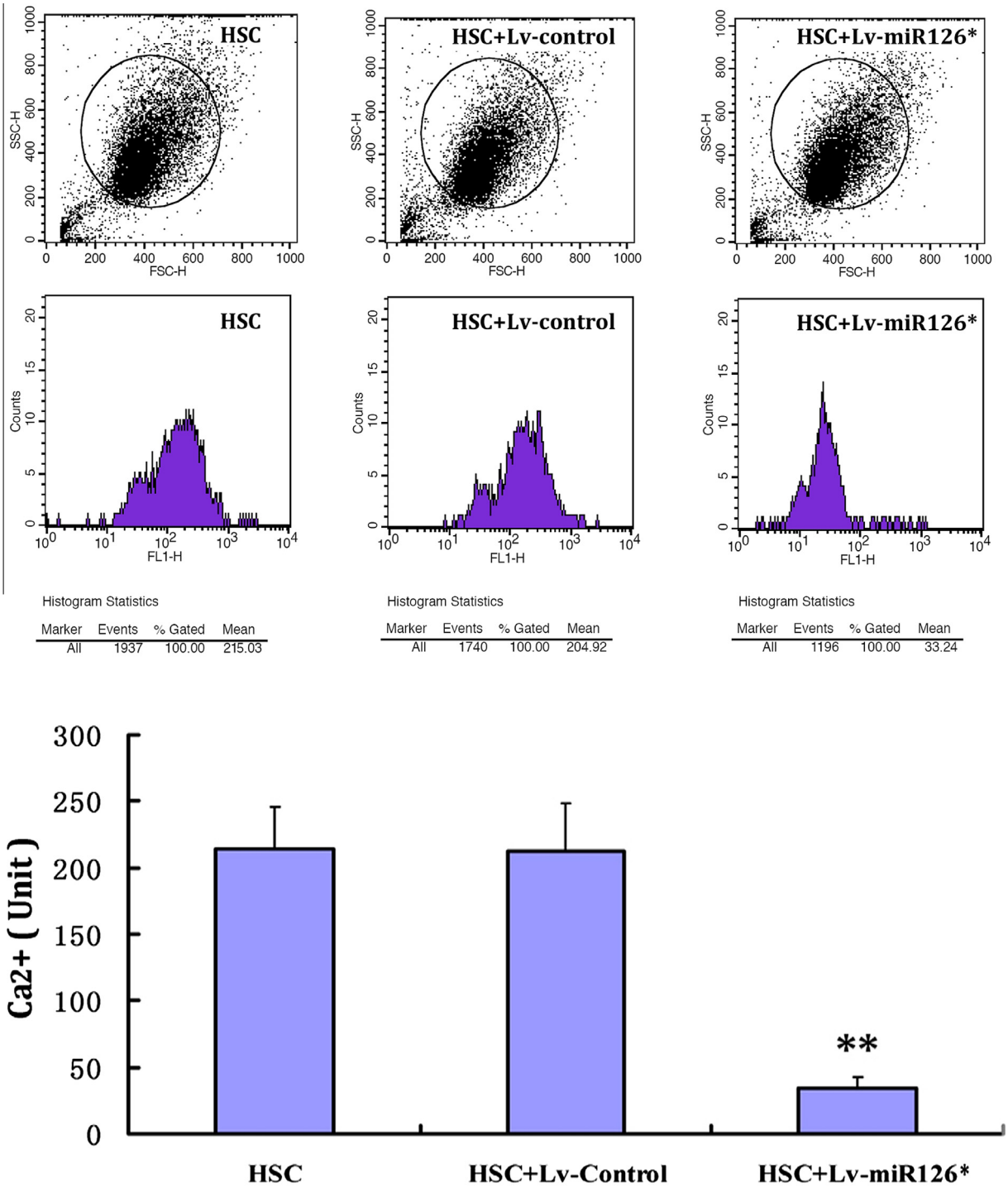

Fig. 8. Intracellular calcium concentrations in HSCs detected by flow cytometry: untransfected group (215.03); control group (204.92); LV-miR-126* group (33.24). Restoring the intracellular miRNAs by miR-126* administration greatly decreased the intracellular calcium concentration in HSCs. $^{**}P < 0.01$ versus corresponding control using Student's *t* test.

(insulin receptor substrate), p85 , PI3K, akt, and Crk. These genes have all been shown to be biological targets of miR-126 [14–20]. Among these target genes, VEGFA, PI3K, AKT and CCND1 within the our previous miRNA-gene networks, which had the highest ratio and enrichment in the VEGF-related pathway, were noted [6]. VEGF-A, which is detected at a low level in quiescent HSCs, is overexpressed in culture-activated HSCs and intrahepatic HSCs after liver injury [20,21]. Recent studies showed early proliferative responses in HSC activation, and the contractile nature of the HSCs was mainly mediated by VEGF pathways [22]. In end-stage liver disease, VEGF-mediated HSC activation is considered to be the major ECM producer responsible for fibrogenesis, and is a mechanistic factor in intrahepatic vascular resistance and pressure regulation [22,23]. Furthermore, administration of VEGF blockers significantly decreases intrahepatic vascular resistance in portal hypertensive syndrome [24]. Using bioinformatics tools, we found that miR-126* was the only miRNA targeting VEGF-A with 7 complementary nucleotides. Moreover, the level of miR-126* was inversely

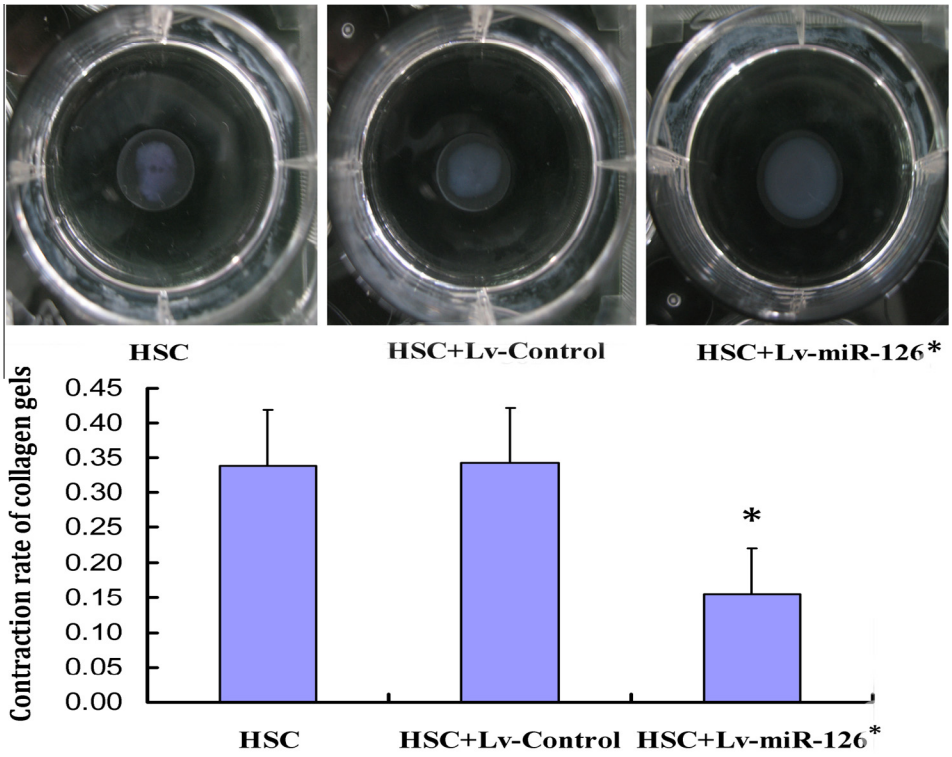

Fig. 9. Contraction of hydrated collagen gels induced by cultured stellate cells. Lv-miR-126* addition to the medium significantly inhibited the contraction of collagen gels. *$P < 0.05$ versus corresponding control using Student's t test.

Table 2
Effect of miR-126* targeting VEGFA on HA, LN, PC III and COL IV.

	HA (ng/ml)	LN (ng/ml)	PC III (ng/ml)	COL IV (ng/ml)
Blank	(70.3 ± 3.6)%	(54.5 ± 3.4)%	(42.1 ± 3.1)%	(32.4 ± 2.3)%
Lv-GFP	(75.3 ± 3.0)%	(53.3 ± 2.7)%	(46.2 ± 2.3)%	(34.2 ± 4.3)%
*Lv-miR-126**	(20.9 ± 4.8)%#	(21.8 ± 5.4)%#	(11.9 ± 3.3)%#	(12.1 ± 4.2)%#

# Indicates P values < 0.01 between blank and *Lv-miR-126**.

correlated with that of VEGF-A in the transformation of HSCs both in vitro and in vivo, which was also in agreement with earlier studies in other tumor lines [25]. miR-126* likely plays important roles in the proliferation and contraction of HSCs by targeting VEGF-A.

Our findings were consistent with these predictions. The VEGF-A/PI3K/AKT pathway had a critical role in the activation of HSCs, and VEGF-A was detected at the protein and mRNA levels in activated rather than quiescent HSCs. Moreover, restored miR-126* greatly reduced VEGF-A, but not VEGF-A mRNA, and the luciferase activity of VEGF-A 3′UTR-based reporter construct in HSCs. Thus, VEGF-A was indicated to be a direct target of miR-126*. As a result, downstream target genes such as VEGF-A (PI3K, p-AKT, CCND1) were inactivated, followed by decreased cytosolic free Ca^{2+}, which is considered to be associated with HSC proliferation and contraction [26,27]. A combination of CCK8 and flow cytometry confirmed marked cell cycle arrest in miR-126*-treated activated HSCs. This provides the first evidence that restoration of the level of miR-126* induces G0/G1 phase arrest in HSCs with a myofibroblast-like phenotype, partially by regulating the Vegf/PI3k/Akt/CCND1 pathway. Besides, during fibrosis progression and portal hypertension, ECM accumulation and activated HSC contraction are key triggering factors [22]. Our results suggest that miR-126* interplays with the Vegf/PI3k/Akt/CCND1 pathway and VEGF-A/Ca^{2+} pathway, thereby blocking ECM accumulation and contraction of HSCs, respectively.

Regulation of the biological behavior of HSCs is a complex process. Increasing evidence indicates that there are other miRNAs, related target genes and pathways involved in cell biological processes other than miR-126* and its induced pathway, such as miR-181b and miR-150 [28,29], but they were not in our miRNA gene network-related pathways. However, it is likely that there may be other miRNAs relevant to the biological changes in HSCs.

In conclusion, our results show that miR-126* may participate in the regulation of HSC contractility and proliferation in chronic liver diseases, partially by targeting the VEGF-mediated signaling pathway. These findings may not only highlight the essence of intrahepatic vascular resistance due to liver diseases, but also facilitate novel therapeutic strategies against portal hypertension and offer insight into its progression.

Acknowledgements

This work is supported by National Natural Science Foundation of China (81100296, 81270492) and sponsored by Shanghai Rising-Star Program (A type) (13QA1402500).

References

[1] Leuci, D., Pomarico, G., Casucci, N., Fucci, B., D'Alitto, N. and Caldarone, A. (2008) Primary prophylaxis of esophageal variceal bleeding in cirrhotic patients. Recenti Prog. Med. 99, 607–610.

[2] Klein, S. et al. (2012) HSC-specific inhibition of Rho-kinase reduces portal pressure in cirrhotic rats without major systemic effects. J. Hepatol. 57, 1220–1227.
[3] Bai, T., Lian, L.H., Wu, Y.L., Wan, Y. and Nan, J.X. (2013) Thymoquinone attenuates liver fibrosis via PI3K and TLR4 signaling pathways in activated hepatic stellate cells. Int. Immunopharmacol. 15, 275–281.
[4] Jiang, J., Ge, X., Li, Z., Wang, Y., Song, Q., Stanley, D.W., Tan, A. and Huang, Y. (2013) MicroRNA-281 regulates the expression of ecdysone receptor (EcR) isoform B in the silkworm, Bombyx mori. Insect Biochem. Mol. Biol. 43, 692–700.
[5] Guo, C.J., Pan, Q., Li, D.G., Sun, H. and Liu, B.W. (2009) MiR-15b and miR-16 are implicated in activation of the rat hepatic stellate cell: an essential role for apoptosis. J. Hepatol. 50, 766–778.
[6] Guo, C.J., Pan, Q., Cheng, T., Jiang, B., Chen, G.Y. and Li, D.G. (2009) Changes in microRNAs associated with hepatic stellate cell activation status identify signaling pathways. FEBS J. 276, 5163–5176.
[7] Guo, C.J., Pan, Q., Jiang, B., Chen, G.Y. and Li, D.G. (2009) Effects of upregulated expression of microRNA-16 on biological properties of culture-activated hepatic stellate cells. Apoptosis 14, 1331–1340.
[8] Friedman, S.L. and Roll, F.J. (1987) Isolation and culture of hepatic lipocytes, Kupffer cells, and sinusoidal endothelial cells by density gradient centrifugation with Stractan. Anal. Biochem. 161, 207–218.
[9] Ishak, K. et al. (1995) Histological grading and staging of chronic hepatitis. J. Hepatol. 22, 696–699.
[10] Saxena, N.K., Titus, M.A., Ding, X., Floyd, J., Srinivasan, S., Sitaraman, S.V. and Anania, F.A. (2004) Leptin as a novel profibrogenic cytokine in hepatic stellate cells: mitogenesis and inhibition of apoptosis mediated by extracellular regulated kinase (Erk) and Akt phosphorylation. FASEB J. 18, 1612–1614.
[11] Dooley, S., Hamzavi, J., Ciuclan, L., Godoy, P., Ilkavets, I., Ehnert, S., Ueberham, E., Gebhardt, R., Kanzler, S., Geier, A., et al. (2008) Hepatocyte-specific Smad7 expression attenuates TGF-beta-mediated fibrogenesis and protects against liver damage. Gastroenterology 135, 642–659.
[12] Yan, M., Zhu, P., Liu, H.M., Zhang, H.T. and Liu, L. (2007) Ethanol induced mitochondria injury and permeability transition pore opening: role of mitochondria in alcoholic liver disease. World J. Gastroenterol. 13, 2352–2356.
[13] Rockey, D.C. and Weisiger, R.A. (1996) Endothelin induced contractility of stellate cells from normal and cirrhotic rat liver: implications for regulation of portal pressure and resistance. Hepatology 24, 233–240.
[14] Meister, J. and Schmidt, M.H. (2010) MiR-126 and miR-126*: new players in cancer. ScientificWorldJournal 10, 2090–2100.
[15] Zhang, J., Du, Y.Y., Lin, Y.F., Chen, Y.T., Yang, L., Wang, H.J. and Ma, D. (2008) The cell growth suppressor, miR-126, targets IRS-1. Biochem. Biophys. Res. Commun. 377, 136–140.
[16] Huang, F., Fang, Z.F., Hu, X.Q., Tang, L., Zhou, S.H. and Huang, J.P. Overexpression of miR-126 promotes the differentiation of mesenchymal stem cells toward endothelial cells via activation of PI3K/Akt and MAPK/ERK pathways and release of paracrine factors. Biol Chem. 394, 1223–1233.
[17] Felli, N. et al. (2013) MiR-126&126* restored expressions play a tumor suppressor role by directly regulating ADAM9 and MMP7 in melanoma. PLoS ONE 8, e56824.
[18] Feng, R. et al. (2010) MiR-126 functions as a tumour suppressor in human gastric cancer. Cancer Lett. 298, 50–63.
[19] Nikolic, I., Plate, K.H. and Schmidt, M.H. (2010) EGFL7 meets miRNA-126: an angiogenesis alliance. J. Angiogenes Res. 2, 9.
[20] Liu, Y. et al. (2009) PTK787/ZK22258 attenuates stellate cell activation and hepatic fibrosis in vivo by inhibiting VEGF signaling. Lab. Invest. 89, 209–221.
[21] Tu, C.T., Guo, J.S., Wang, M. and Wang, J.Y. (2007) Antifibrotic activity of rofecoxib in vivo is associated with reduced portal hypertension in rats with carbon tetrachloride-induced liver injury. J. Gastroenterol. Hepatol. 22, 877–884.
[22] Thabut, D. and Shah, V. (2010) Intrahepatic angiogenesis and sinusoidal remodeling in chronic liver disease: new targets for the treatment of portal hypertension? J. Hepatol. 53, 976–980.
[23] Liang, J., Deng, X., Lin, Z.X., Zhao, L.C. and Zhang, X.L. (2009) Attenuation of portal hypertension by natural taurine in rats with liver cirrhosis. World J. Gastroenterol. 15, 4529–4537.
[24] Fernandez, M., Mejias, M., Garcia-Pras, E., Mendez, R., Garcia-Pagan, J.C. and Bosch, J. (2007) Reversal of portal hypertension and hyperdynamic splanchnic circulation by combined vascular endothelial growth factor and platelet-derived growth factor blockade in rats. Hepatology 46, 1208–1217.
[25] Liu, B., Peng, X.C., Zheng, X.L., Wang, J. and Qin, Y.W. (2009) MiR-126 restoration down-regulate VEGF and inhibit the growth of lung cancer cell lines in vitro and in vivo. Lung Cancer 66, 169–175.
[26] Takahashi, M., Matsui, A., Inao, M., Mochida, S. and Fujiwara, K. (2003) ERK/MAPK-dependent PI3K/Akt phosphorylation through VEGFR-1 after VEGF stimulation in activated hepatic stellate cells. Hepatol. Res. 26, 232–236.
[27] Oide, H., Itatsu, T., Hirose, M., Wang, X.E., Nishiyama, D., Takei, Y. and Sato, N. (2000) Acute and chronic effect of alcohol on Ca^{2+} channels in hepatic stellate cells. Alcohol. Clin. Exp. Res. 24, 357–360.
[28] Wang, B., Li, W., Guo, K., Xiao, Y., Wang, Y. and Fan, J. (2012) MiR-181b promotes hepatic stellate cells proliferation by targeting p27 and is elevated in the serum of cirrhosis patients. Biochem. Biophys. Res. Commun. 421, 4–8.
[29] Venugopal, S.K., Jiang, J., Kim, T.H., Li, Y., Wang, S.S., Torok, N.J., Wu, J. and Zern, M.A. (2010) Liver fibrosis causes downregulation of miRNA-150 and miRNA-194 in hepatic stellate cells, and their overexpression causes decreased stellate cell activation. Am. J. Physiol. Gastrointest. Liver Physiol. 298, G101–6.